

file: (A) : *Wang* (51)

Phase Control of HF Chemical Lasers for Coherent Recombination

Prepared by C. P. WANG
Aerophysics Laboratory
The Ivan A. Getting Laboratories
and
P. L. SMITH
Control Analysis Department
Guidance and Control Division

16 October 1978

Prepared for
VICE PRESIDENT AND GENERAL MANAGER
THE IVAN A. GETTING LABORATORIES



The Ivan A. Getting Laboratories
THE AEROSPACE CORPORATION
PLEASE RETURN TO:

BMD TECHNICAL INFORMATION CENTER
BALLISTIC MISSILE DEFENSE ORGANIZATION
7100 DEFENSE PENTAGON
WASHINGTON D.C. 20301-7100

19980309 291

DISTRIBUTION STATEMENT A

Approved for public release;
Distribution Unlimited

INFO QUALITY INSURED

U4014

THE IVAN A. GETTING LABORATORIES

The Laboratory Operations of The Aerospace Corporation is conducting experimental and theoretical investigations necessary for the evaluation and application of scientific advances to new military concepts and systems. Versatility and flexibility have been developed to a high degree by the laboratory personnel in dealing with the many problems encountered in the nation's rapidly developing space and missile systems. Expertise in the latest scientific developments is vital to the accomplishment of tasks related to these problems. The laboratories that contribute to this research are:

Aerophysics Laboratory: Launch and reentry aerodynamics, heat transfer, reentry physics, chemical kinetics, structural mechanics, flight dynamics, atmospheric pollution, and high-power gas lasers.

Chemistry and Physics Laboratory: Atmospheric reactions and atmospheric optics, chemical reactions in polluted atmospheres, chemical reactions of excited species in rocket plumes, chemical thermodynamics, plasma and laser-induced reactions, laser chemistry, propulsion chemistry, space vacuum and radiation effects on materials, lubrication and surface phenomena, photosensitive materials and sensors, high precision laser ranging, and the application of physics and chemistry to problems of law enforcement and biomedicine.

Electronics Research Laboratory: Electromagnetic theory, devices, and propagation phenomena, including plasma electromagnetics; quantum electronics, lasers, and electro-optics; communication sciences, applied electronics, semiconducting, superconducting, and crystal device physics, optical and acoustical imaging; atmospheric pollution; millimeter wave and far-infrared technology.

Materials Sciences Laboratory: Development of new materials; metal matrix composites and new forms of carbon; test and evaluation of graphite and ceramics in reentry; spacecraft materials and electronic components in nuclear weapons environment; application of fracture mechanics to stress corrosion and fatigue-induced fractures in structural metals.

Space Sciences Laboratory: Atmospheric and ionospheric physics, radiation from the atmosphere, density and composition of the atmosphere, aurorae and airglow; magnetospheric physics, cosmic rays, generation and propagation of plasma waves in the magnetosphere; solar physics, studies of solar magnetic fields; space astronomy, x-ray astronomy; the effects of nuclear explosions, magnetic storms, and solar activity on the earth's atmosphere, ionosphere, and magnetosphere; the effects of optical, electromagnetic, and particulate radiations in space on space systems.

THE AEROSPACE CORPORATION
El Segundo, California

Accession Number: 4014

Publication Date: Oct 16, 1978

Title: Phase Control of HF Chemical Lasers for Coherent Recombination

Personal Author: Wang, C.P.; Smith, P.L.

Corporate Author Or Publisher: Aerospace Corporation, El Segundo, CA 90245 Report Number: ATR-78(8408)-2

Report Prepared for: Space and Missile Systems Organization, Air Force Systems Command, Los Angeles, CA Report Number Assigned by Contract Monitor: SLL 80 126

Comments on Document: Archive, RRI, DEW

Descriptors, Keywords: Phase Control Hydrogen Fluoride HF Chemical Laser Coherent Recombination Servo System Optics Frequency Drift Piezoelectric Transducer Mirror Expression Vector Covariance

Pages: 00047

Cataloged Date: Dec 07, 1992

Contract Number: F04701-77-C-0078

Document Type: HC

Number of Copies In Library: 000001

Record ID: 25484

Source of Document: DEW

PHASE CONTROL OF HF CHEMICAL LASERS
FOR COHERENT RECOMBINATION

Prepared by

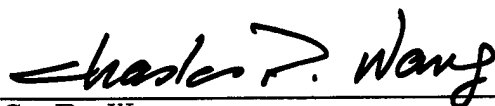
C. P. Wang
Aerophysics Laboratory
The Ivan A. Getting Laboratories
and
P. L. Smith
Control Analysis Department
Guidance and Control Division

16 October 1978

The Ivan A. Getting Laboratories
THE AEROSPACE CORPORATION
El Segundo, Calif. 90245

PHASE CONTROL OF HF CHEMICAL LASERS
FOR COHERENT RECOMBINATIONS

Prepared



C. P. Wang
Aerophysics Laboratory

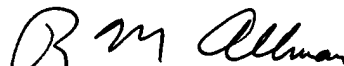


P. L. Smith
Guidance and Control Division

Approved



H. Mirels, Head
Aerodynamics and Heat Transfer
Department



R. M. Allman, Director
Control Analysis Department
Guidance and Control Division



W. R. Warren, Jr., Director
Aerophysics Laboratory
The Ivan A. Getting Laboratories

ABSTRACT

A servo system for phase-locking two HF chemical lasers, operated on selected lines, has been designed and simulated. A steady-state phase error is achieved that is adequate for coherent optical recombination. The results are based on the measured frequency drift of a small HF chemical laser and the measured frequency response of a piezoelectric transducer (PZT) mirror driver. A major innovation is the use of rate feedback with a laser Doppler sensor to extend the useful frequency response of the PZT driver. Closed-form expressions for the regulator gains derived by quadratic synthesis and state vector covariance are provided.

CONTENTS

ABSTRACT	v
I. INTRODUCTION	1
II. HF CHEMICAL LASERS	3
III. PZT DRIVER	7
IV. SERVO DESIGN BY QUADRATIC SYNTHESIS	9
V. IMPLEMENTATION OF RATE FEEDBACK	17
VI. SERVO-TRACKING-ERROR COVARIANCE ANALYSIS	23
VII. SIMULATION RESULTS	25
VIII. CONCLUSION	33
REFERENCES	35
APPENDIXES:	
A. QUADRATIC SYNTHESIS OF FEEDBACK REGULATOR	37
B. STEADY-STATE COVARIANCE OF STATE VECTOR ...	43

FIGURES

1.	Block Diagram of Phase-Control Loop	2
2.	Frequency Drift of Free-Running Chemical Laser	4
3.	State Feedback Regulator	11
4.	Feedback Gains Versus Phase-Error Weighting Coefficient	13
5.	Phase Regulator in Classical Form	14
6.	Physical Elements of Servo System	16
7.	PZT Driver with Laser Doppler Sensor and Rate Feedback	18
8.	Simulated Step Response of PZT Driver With and Without Rate Feedback	20
9.	Linearized RMS Phase Error Versus Phase-Error Weighting Coefficient	24
10.	Phase Error	26
11.	PZT Displacement	27
12.	PZT Displacement Rate	28
13.	Laser Frequency Shift	29
14.	Frequency Tracking Error	30

I. INTRODUCTION

The major optical problems for high-power lasers are efficient power extraction and handling and control of such laser beams with adequate beam quality and stability. A technique for coherent optical recombination of several laser beams may have to be developed to solve these problems. For the coherent optical recombination of such laser beams as the master and slave oscillator array (MASOA) system^{1, 2} and for such laser-frequency phase-control systems as the coherent optical adaptive technique (COAT)³ and laser frequency stabilization schemes,⁴⁻⁶ a wide bandwidth phase-control system is required.

The following critical issues for the phase-control of HF chemical lasers operating on selected lines were examined: (1) What is the frequency drift of HF chemical lasers? (2) What is the response of available piezo-electric transducer (PZT) mirror drivers? (3) Can a servo be designed to phase-lock HF chemical lasers?

The frequency drift of a small HF chemical laser^{5, 7} and the frequency response of a PZT mirror driver were measured, and models were fitted to the experimental data.

A phase-control servo was designed by means of the quadratic synthesis technique.^{8, 9} Figure 1 is a simplified block diagram of the servo. A major innovation is the use of rate feedback with a laser Doppler sensor¹⁰ used on the mirror face to increase the useful PZT frequency response^{11, 12} and reduce the effects of nonlinearities.

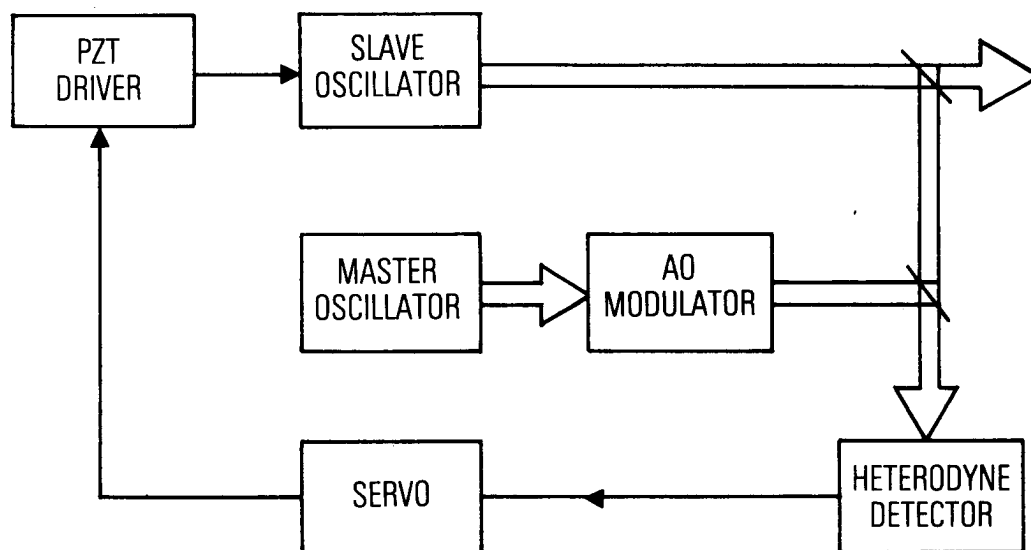


Fig. 1. Block Diagram of Phase-Control Loop

II. HF CHEMICAL LASERS

The cw HF(DF) chemical laser^{7, 13} is a potential high-efficiency, high-power gas laser, but its gain medium is complicated by the nature of the chemical reaction and the rotation-vibration transitions, medium nonuniformity, and mixed inhomogeneous and homogeneous behavior.^{14, 15} The frequency stability of a free-running cw HF chemical laser is rather poor, on the order of 30 MHz.⁵ It is necessary to determine the frequency drift of the laser to estimate the performance of the servo loop.

Experiments were carried out with a cw HF chemical laser operating on a single line. The laser used is described in an earlier paper.^{5, 7} Briefly, F atoms are generated by a discharge in a gas mixture of He, O₂, and SF₆. The latter is mixed with H₂, which is injected just upstream of a transverse optical cavity. The cavity pressure could vary from 5 to 15 Torr. Typical single-line output at 2.87 μm is 0.5 W. The gain medium is 10 cm long, and there is a small signal gain of about 0.05 cm⁻¹.

A stable resonator was used that had a 2-m radius-of-curvature total reflector (reflectivity > 95%) and a flat grating (reflectivity 80%) as the output coupling. The resonator and coupling were separated by a distance of 150 cm; hence, the empty cavity mode spacing was 100 MHz. A TEM₀₀-mode output beam was obtained by means of a variable aperture inside the resonator. The totally reflecting mirror was mounted on a PZT driver, which could move the mirror and scan the laser frequency across the gain

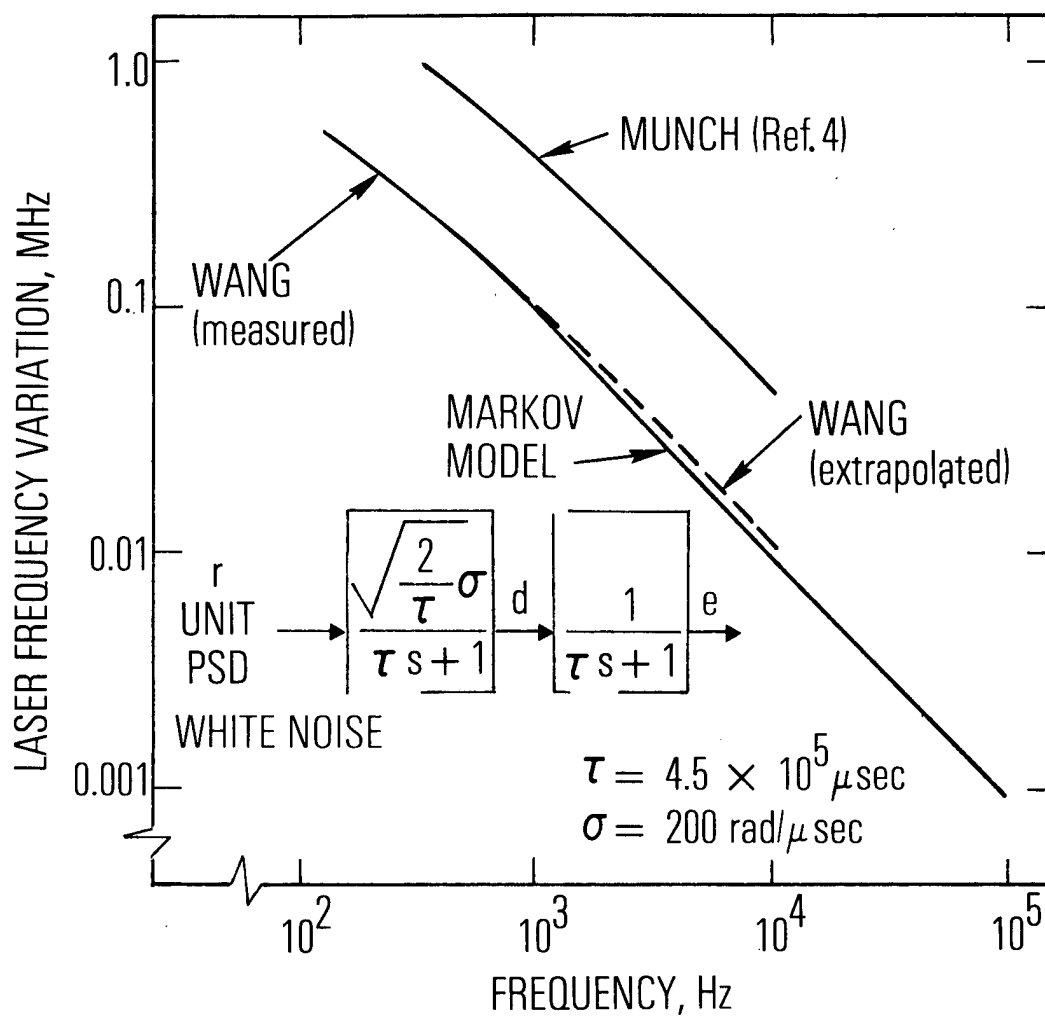


Fig. 2. Frequency Drift of Free-Running Chemical Laser

linewidth. An InAs fast detector and a Hewlett-Packard spectrum analyzer with a plug-in 8553B unit were used to analyze the beat-frequency spectrum. A 25-cm Fabry-Perot confocal interferometer also was used to measure the frequency drift spectrum of the laser (Fig. 2). Frequency drift above 1000 Hz is obtained by extrapolating the measured data. The measured frequency drift was close to but somewhat lower than that measured in Ref. 4. The difference may be the result of our optics being mounted on a vibration-isolated optical table (Newport Research Corporation).

The frequency drift is modeled by a second-order Gaussian Markov random process with cascaded lag filter time constants τ and steady-state fluctuation root-mean-square (RMS) σ . Values of $\tau = 4.5 \times 10^5 \mu\text{sec}$ and $\sigma = 200 \text{ rad}/\mu\text{sec}$ fit the measured and extrapolated frequency drift shown in Fig. 2 very well.

III. PZT DRIVER

The frequency of the lowest order resonance mode for a thin disk-shaped piezoelectric transducer (PZT) driving a mirror of mass m , which is much larger than the mass of the PZT driver, is approximately

$$\omega_n = \sqrt{\frac{k}{m}} = \sqrt{\frac{\pi D^2 Y}{4hm}} \quad (1)$$

where k , D , h , and Y are the equivalent spring constant, diameter, thickness, and Young's modulus of the PZT driver, respectively. Higher order modes may involve the moment of inertia of the PZT driver. The displacement Δh of the PZT driver is

$$\Delta h = d_{33} E h \quad (2)$$

where d_{33} is the piezoelectric constant, and E is the applied electric field strength. For high-frequency response, h and m should be as small as possible. The thickness is limited by the required maximum displacement and the maximum electric breakdown voltage or maximum electric-field strength.

The mechanical response of the PZT and mirror is modeled by a second-order transfer function

$$H(s) = \frac{\omega_n^2}{s^2 + 2\zeta\omega_n s + \omega_n^2} \quad (3)$$

where ω_n is the resonance frequency, and ζ is the damping coefficient. For a typical PZT mirror driver, well within the state of the art,

$\omega_n = 0.03 \text{ rad}/\mu\text{sec}$ (5 kHz) and $\zeta = 0.6$. Because of excessive PZT phase lag, the frequency response of a simple single-loop positioning servo is limited to about 3 kHz — not high enough to follow the laser frequency variations and maintain phase lock. A more sophisticated servo design is required.

IV. SERVO DESIGN BY QUADRATIC SYNTHESIS

Servo design for linear, multivariable systems is well developed.^{8,9,11} Linearization of nonlinear systems makes linear design methods widely applicable, particularly to laser phase control.

In the results reported here the uncertainty in models and signals is ignored, and a range of gains is investigated to determine the relationships of the PZT bandwidth, laser drift, and the phase error. Additional analysis is required to specify the necessary signal-to-noise ratios of the loop elements to ensure that the performance of the idealized, deterministic design can be achieved.

The quadratic synthesis method was used to design the phase-control system. The quadratic synthesis approach is preferred to other linear synthesis techniques such as the frequency-domain and root-locus methods, pole-placement, and compensator parameter optimization^{8,9} because the complexities of more detailed models and multiple PZT drivers can be analyzed in a progressive manner by means of the same basic approach.

Quadratic-control-system synthesis always results in a stable system,¹² although some designs may require unrealistically high gains or result in actuator excursions outside the allowable dynamic range or valid model linearization region. Hence experience and caution are required in interpreting the results, and a simulation is used to verify the design.

Models of the PZT, laser frequency drift, phase detector, and state feedback loop are shown in Fig. 3. It is assumed that the lasers are locked and that the approximation $\sin \theta \approx \theta$ is valid in order to compute the regulator gains. The electrical response of the PZT is not explicitly modeled;¹² it is assumed that the amplifier can supply the necessary driving voltage and current without saturating and that the amplifier transient response is not a limiting factor. There are five state variables: θ is the linearized phase error (radians), y is frequency shift in the slave laser caused by PZT displacement (rad/ μ sec), v is the time derivative of y , and d and e are the state variables used to model the relative frequency shift between the two lasers that results from drift (rad/ μ sec).

In quadratic synthesis all the state variables are multiplied by gains and summed to form the error signal (Fig. 3). Not all state variables are directly measured in the actual system, and in general an "observer system" is necessary to reconstruct the unmeasured state variables.⁸ Since noise is always present, filtering is necessary to reconstruct smooth estimates of the unmeasured state variables. Filtering will add some phase lag to the loop; hence, it is desirable to provide the highest quality observed signals in order to reduce the filtering lag to a minimum. The state feedback gains $C_1 - C_5$ minimize the average value of the cost functional J ,

$$J = \int [(w\theta)^2 + u^2] dt \quad (4)$$

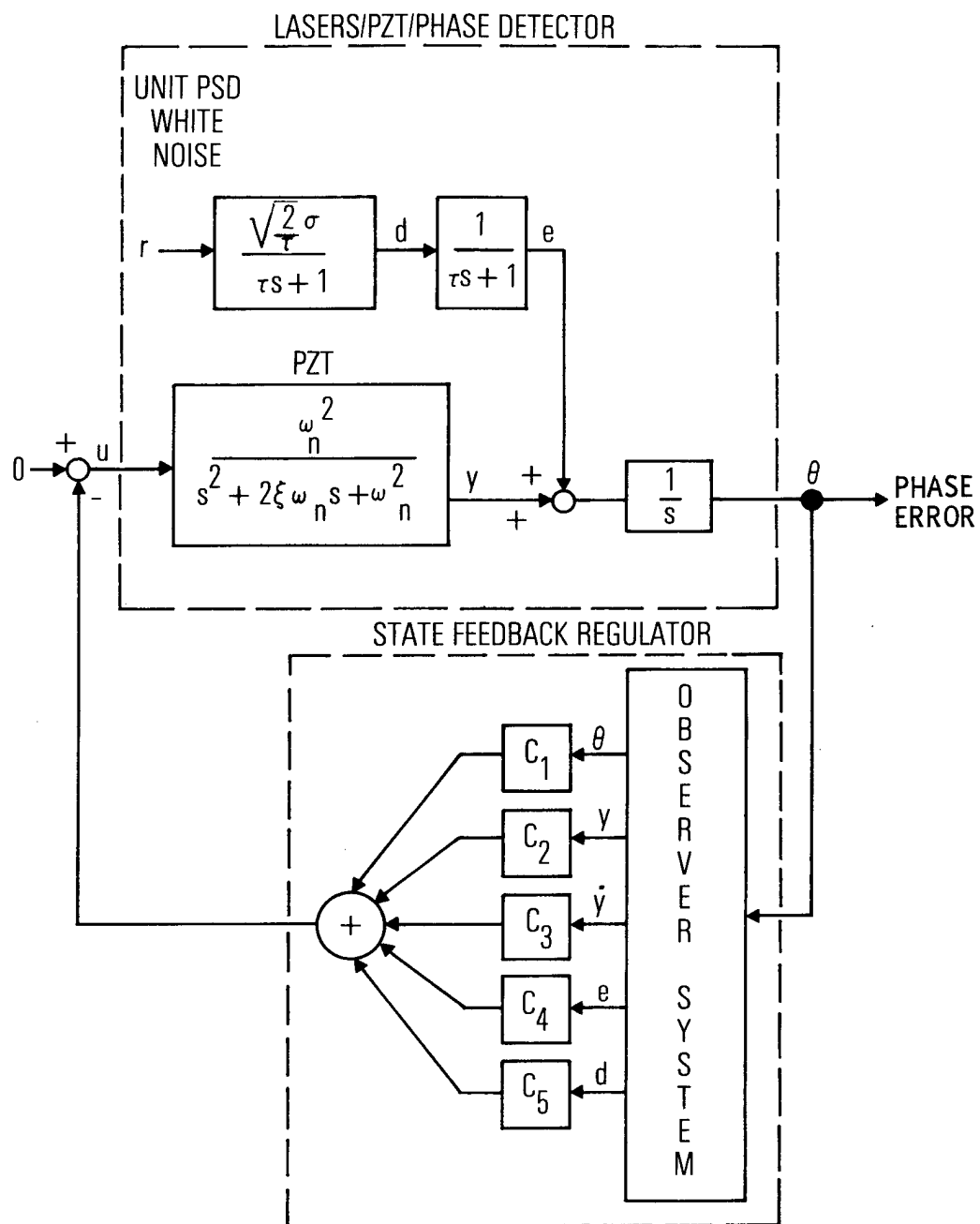


Fig. 3. State Feedback Regulator

where u is the PZT commanded frequency shift, and W is the phase error weighting coefficient. In the quadratic synthesis method W is the parameter that the designer adjusts to achieve the desired response. Increasing W increases the gains and decreases the phase error. There are practical limits on the size of W (and the resultant feedback gains) because of noise, unmodeled nonlinearities and resonance modes, and power limits. The major advantage of the quadratic synthesis method, particularly in a preliminary design study such as this, is that the controller design is a function of only one independent parameter (W).

Preliminary results indicated that the control system could be simplified without an appreciable loss in performance if it is assumed that $C_4 = C_2$ and $C_5 = 0$ (Appendix A). With this approximation the state feedback regulator reduces to the conventional servo-loop architecture for an actuator positioning control system (Fig. 4), i.e., an inner rate stabilized loop and an outer position loop with high-frequency boost compensation. If θ , $\dot{\theta}$, and v are measured directly, no observer system is necessary. Rate feedback is mandatory in conventional precision tracking loops to reduce the phase lag of lightly damped gimbaled masses.^{8, 11} In this application rate feedback reduces the PZT phase lag by increasing the damping, which in turn permits a greater degree of high-frequency boost in the outer position loop. Rate feedback also reduces the effect of nonlinearities in the PZT response, a result that cannot be achieved with outer loop phase lead compensation alone. Figure 5 is a

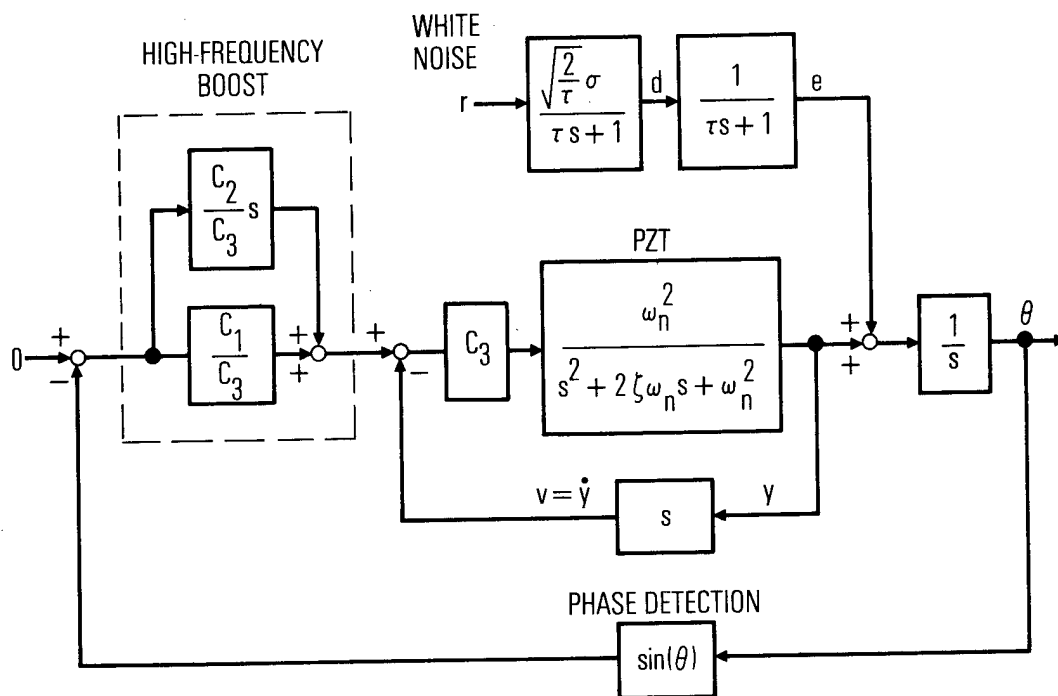


Fig. 4. Feedback Gains Versus Phase-Error Weighting Coefficient

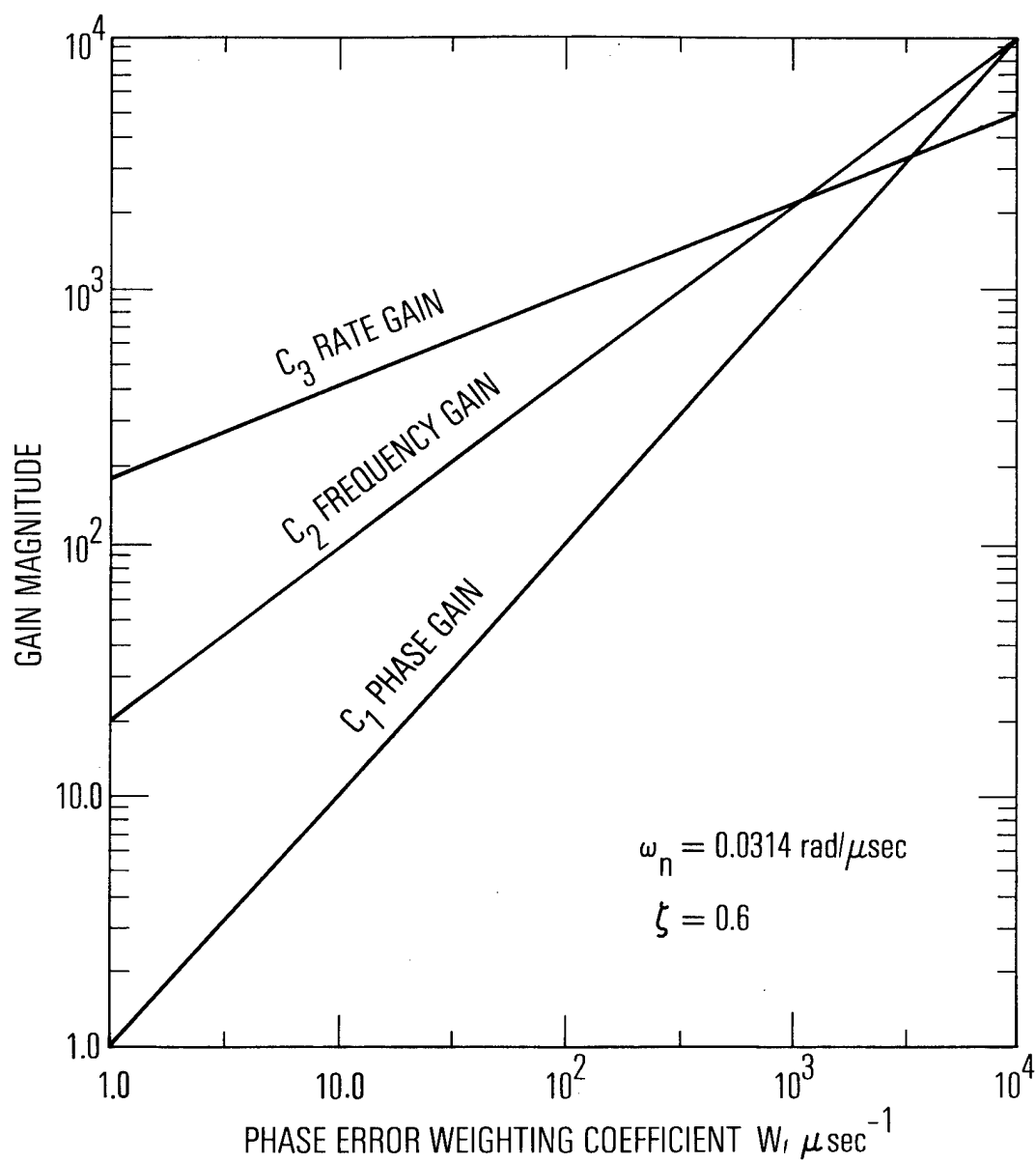


Fig. 5. Phase Regulator in Classical Form

plot of the loop gains as a function of W . The gains are computed by the routine procedure of solving the steady-state Ricatti equation associated with the state equations and the cost functional J .^{8,9}

Figure 6 is a block diagram of the physical elements of the phase control servo.

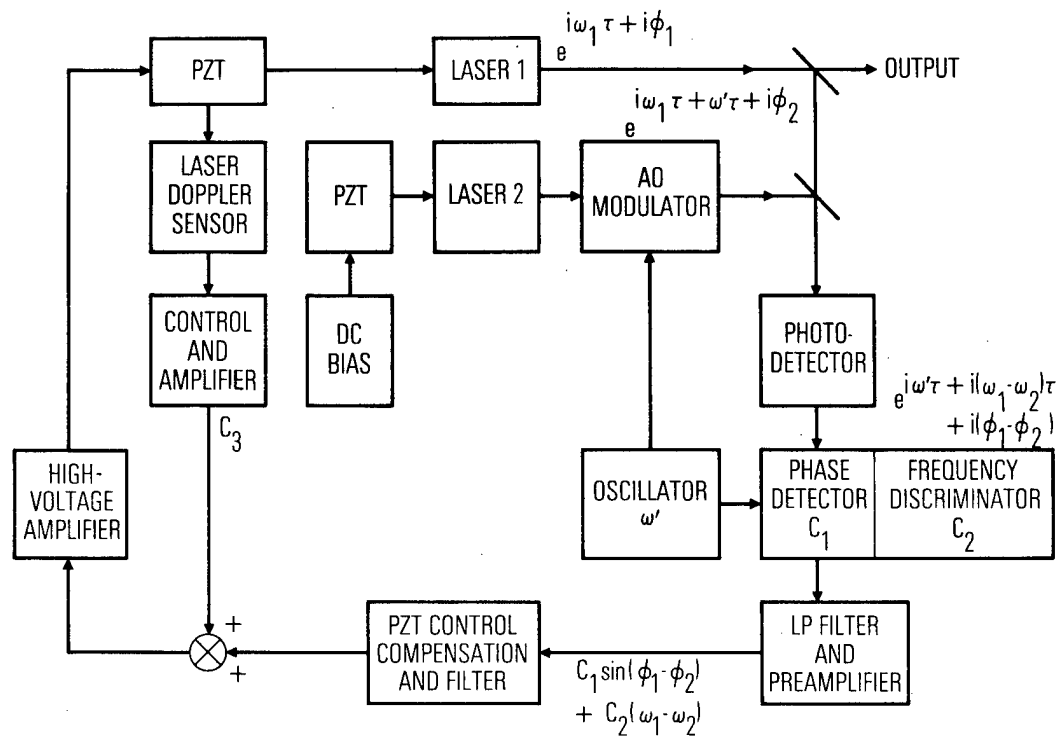


Fig. 6. Physical Elements of Servo System

V. IMPLEMENTATION OF RATE FEEDBACK

A major design problem is to derive the PZT displacement rate signal. Figure 7 is a schematic diagram of the PZT driver with a laser Doppler sensor for measuring the displacement rate.

Laser Doppler velocimeters¹⁰ have been extensively used for velocity measurement. Basically, when light is scattered or reflected from a moving object, its frequency is shifted as a result of the Doppler effect. The frequency shift $\Delta\omega_D$ is related to the velocity \vec{V} by the relation¹⁰

$$\Delta\omega_D = \vec{V} \cdot (\vec{k}_1 - \vec{k}_2) = 2 \frac{V}{c} \omega_L \cos \phi \cos \frac{\psi}{2} \quad (5)$$

where \vec{k}_1 and \vec{k}_2 are the wave vectors of the incident light and scattered light, respectively; c is the speed of light; ϕ is the angle between \vec{V} and $(\vec{k}_1 - \vec{k}_2)$; ψ is the angle between \vec{k}_1 and $-\vec{k}_2$; and ω_L is the frequency of the light source.

For the configuration shown in Fig. 7, both $\cos \phi$ and $\cos \psi/2$ are near 1. For the application here, the mirror velocity is of the order of 10^{-5} m/sec, which corresponds to a frequency shift $\Delta\omega_D$ of 20 Hz. An optical heterodyne and acousto-optical modulation technique is proposed to detect such low frequencies with sufficient bandwidth. As shown in Fig. 7, the laser beam is split by the first beam splitter. The reflected beam is reflected again by the mirror and reaches a second beam splitter. The transmitted beam goes through an acousto-optical modulator, which shifts

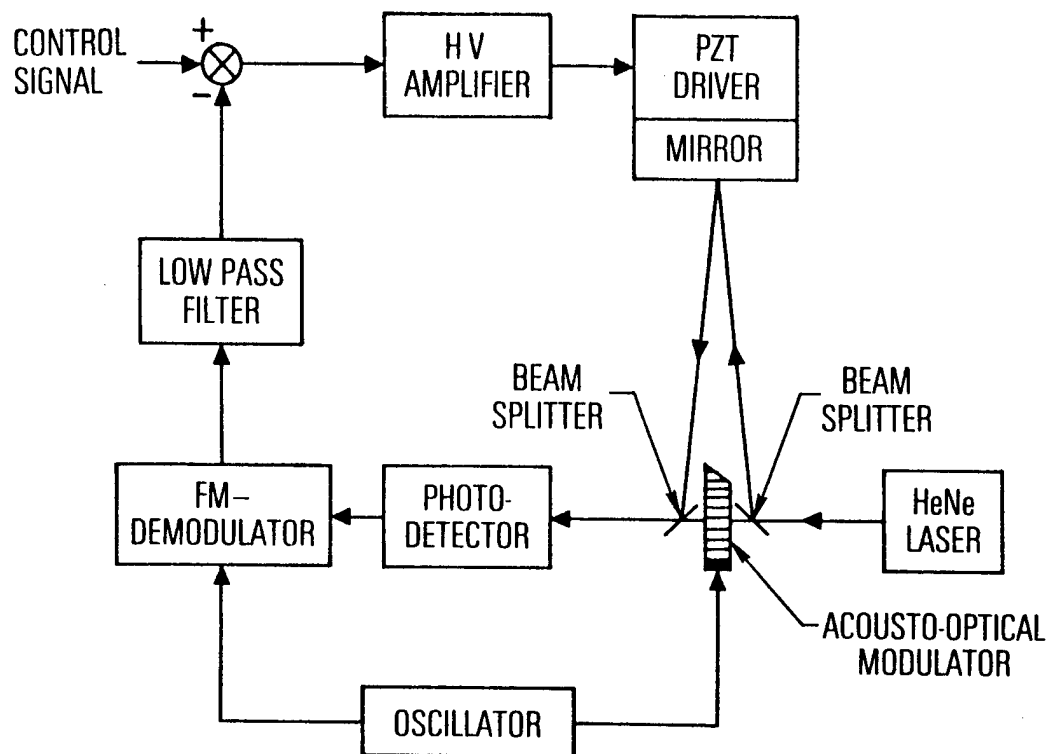


Fig. 7. PZT Driver with Laser Doppler Sensor and Rate Feedback

the laser frequency by a frequency ω_m . Then both beams are combined by the second beam splitter and fall on the photodetector. The detector output is the beat signal $\omega_m \pm \omega_D$.

An fm demodulator with center frequency ω_m is used to detect ω_D . The fm-demodulator output v_D is then proportional to ω_D . This signal is then passed through a low-pass filter, an amplifier, a high-voltage amplifier, and finally fed back to the PZT driver.

For a typical case the center frequency ω_m is 100 kHz with a signal bandwidth of 20 kHz. An fm demodulator with an accuracy of -80 dB is required to detect the 20-Hz modulation. This performance is within reach of present technology.

The inner rate feedback loop transfer function is

$$H_c(s) = \frac{C_3 \omega_n^2}{s^2 + (2\zeta \omega_n + C_3 \omega_n^2)s + \omega_n^2} \quad (6)$$

A comparison of Eqs. (3) and (6) reveals that the rate feedback introduces an active damping force, which reduces the phase lag, which in turn permits a greater degree of high-frequency boost in the outer positioning loop, without causing instability. Furthermore, because of the large rate feedback gain, the effect of nonlinearities in the PZT response is reduced.⁸

The step response of the PZT with and without rate feedback is shown in Fig. 8 for $\omega_n = 0.03$ rad/ μ sec and $\zeta = 0.6$. Note that the PZT response with a rate feedback gain of $C_3 = 421$ μ sec is much faster than the PZT without rate feedback. The response of the inner loop is ultimately limited

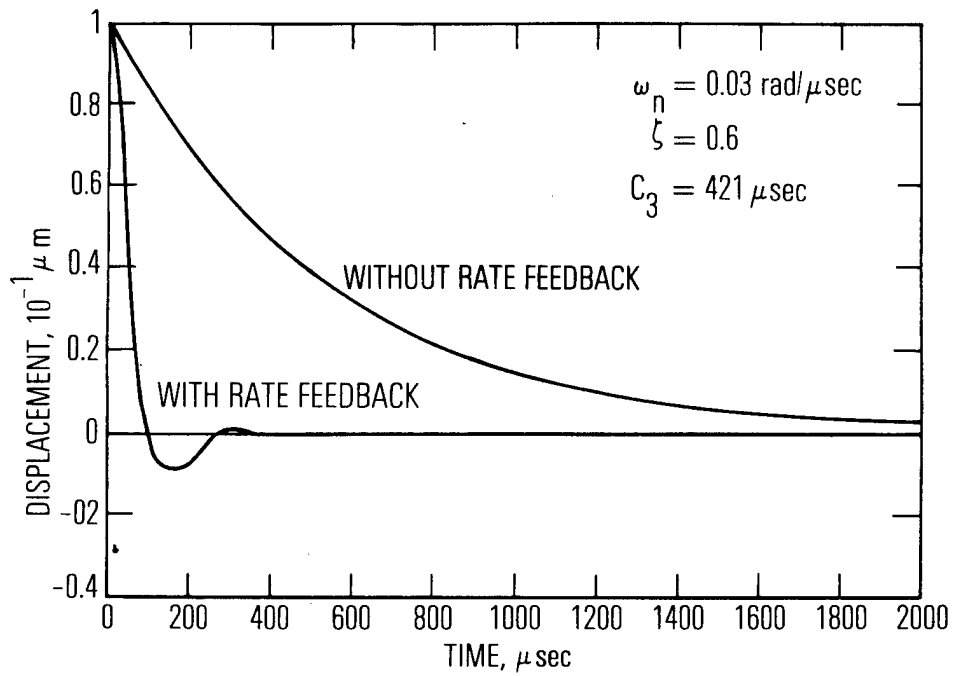


Fig. 8. Simulated Step Response of PZT Driver With and Without Rate Feedback

by the rate sensing noise and higher order structural resonances. How far the PZT response can be extended by the use of rate feedback must be determined experimentally.

VI. SERVO-TRACKING-ERROR COVARIANCE ANALYSIS

The RMS steady-state phase error can be computed as a closed-form function of W and the RMS random frequency drift σ if the approximation $\sin \theta \approx \theta$ is valid. The procedure is described in Ref. 8 and the results are given in Appendix B. Figure 9 is a plot of the RMS phase error versus W for $\omega_n = 0.03$ rad/ μ sec (5 kHz), $\sigma = \sqrt{2} \times 200$ μ sec = 282 μ sec for two lasers), $\tau = 4.5 \times 10^5$ μ sec, and $\zeta = 0.6$. The lower region of the plot (below the dashed line) is valid for the linearized models; above about 0.1 rad the linearizing assumption of $\sin \theta \approx \theta$ may introduce larger error.

For the frequency-drift and PZT parameters considered, i.e., a noise-free control system with feedback gains corresponding to $W = 10^3$ μ sec $^{-1}$, the plot (Fig. 9) indicates that the RMS phase error is about 12 deg.

A single PZT servo may require excessively large excursions. The typical approach is to use a high-gain, low-frequency servo to reduce the large-excursion frequency drift in conjunction with a low-gain, high-frequency servo to remove the residual high-frequency, small-excursion drift. The low-frequency servo presents no design problems; the concern here is with canceling the high-frequency (above 1000 Hz) drift. If it is assumed, for example, that the low-frequency servo reduces the frequency variations below 100 Hz and the residual high-frequency drift is specified by $\sigma = 0.45$ rad/ μ sec and $\tau = 717$ μ sec, the servo gains corresponding to $W = 10$ μ sec $^{-1}$ are then adequate to drive the residual phase error to an RMS value of less than 3 deg (Fig. 9).

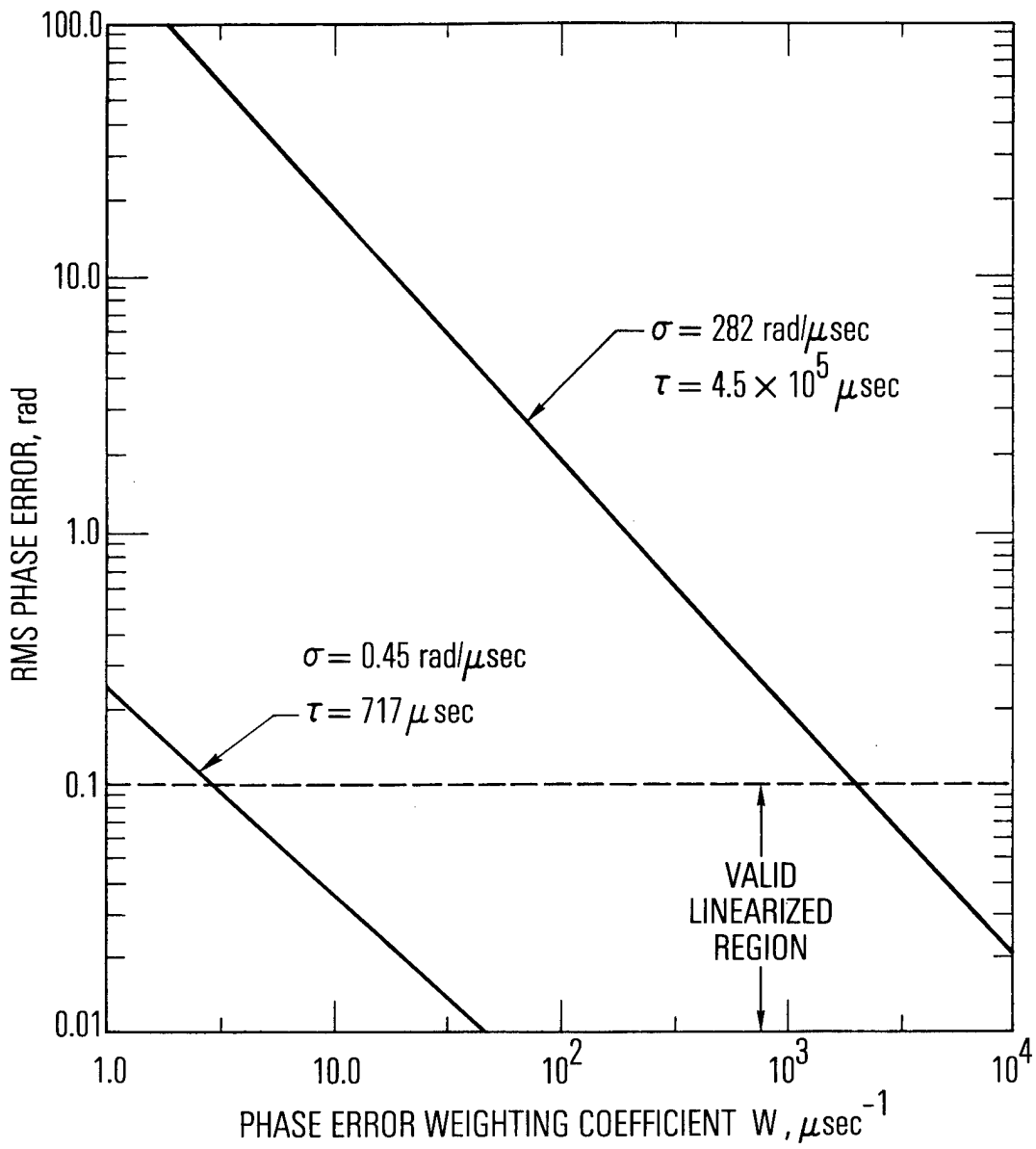


Fig. 9. Linearized RMS Phase Error Versus Phase-Error Weighting Coefficient

VII. SIMULATION RESULTS

The phase-control system in Fig. 4 was simulated on a CDC 7600 computer. Gaussian distributed random numbers were used to simulate the white noise input to the frequency-drift shaping filters. A total of 20 differential equations (5 for the servo and 15 for the linearized covariance analysis) were numerically integrated by means of a fixed-step Runge Kutta algorithm with a step size of $0.5 \mu\text{sec}$ for a period of $2000 \mu\text{sec}$.

Figures 10 to 14 are time-history plots of the state variables with the lasers locked initially ($\theta = 0$) for $\omega_n = 0.03$, $\zeta = 0.6$, $\sigma = 0.45 \text{ rad}/\mu\text{sec}$, $\tau = 7.2 \times 10^2 \mu\text{sec}$, and the gains corresponding to $W = 10 \mu\text{sec}^{-1}$.

The corresponding $1-\sigma$ bounds from the state covariance equations are overlayed on the state variables. Although the covariance analysis is based on the linearized model, the results are valid (signal lies inside bound 67% of the time) when $\sin \theta \simeq \theta$, which is true for this case after lock-up has been achieved.

The transient response is highly nonlinear.¹⁶ A typical case with an initial frequency difference of 10.0 MHz locks in $60 \mu\text{sec}$. Cycle slipping occurs, but phase lock-up is rapidly achieved because of the frequency feedback term in the regulator error signal. The actual lock-up time may be limited by the saturation of the PZT driver amplifier, which was not modeled.

The excellent agreement between the simulation and the linearized covariance analysis simplifies the performance analysis considerably.

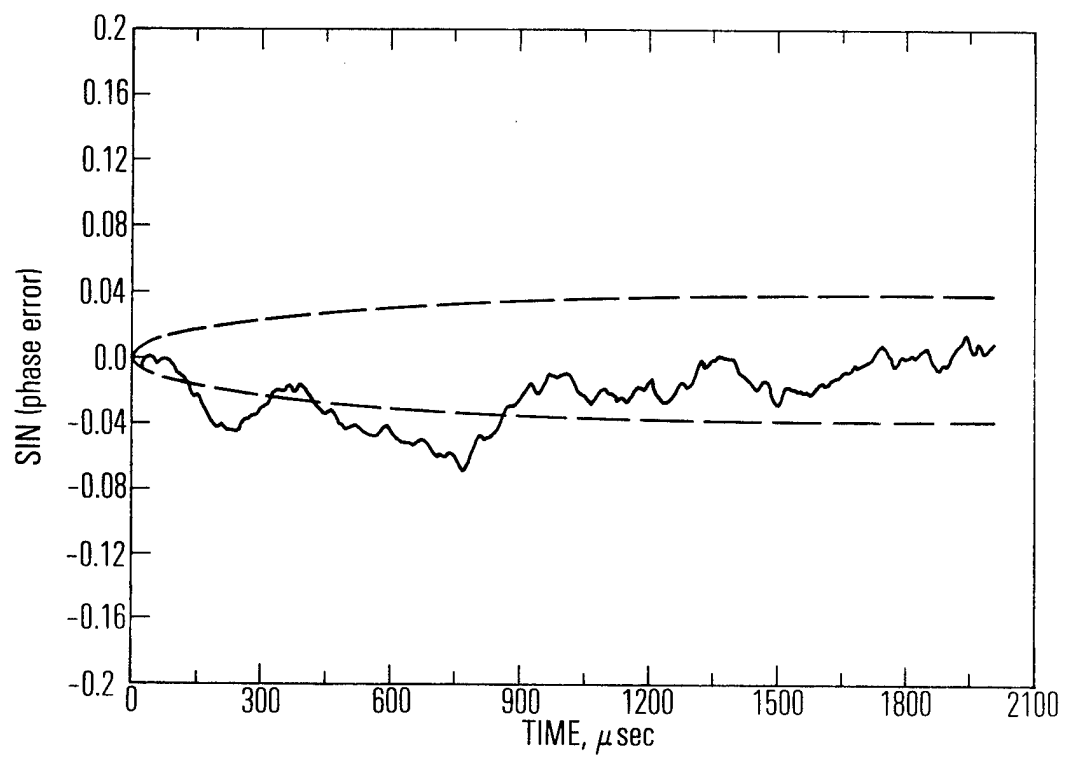


Fig. 10. Phase Error

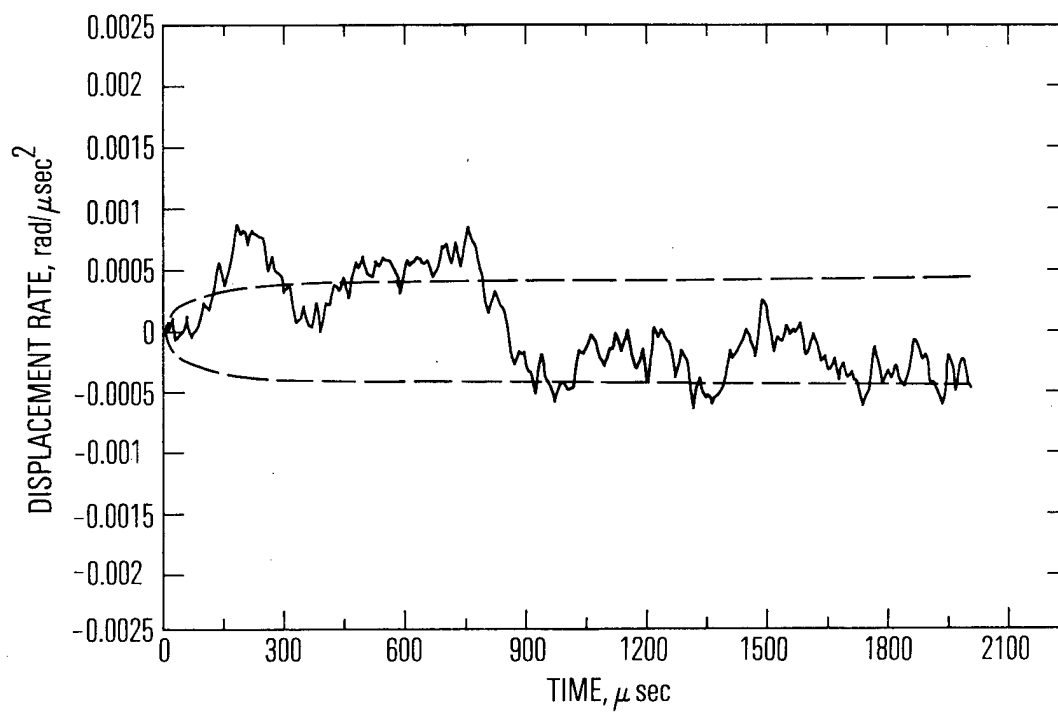


Fig. 11. PZT Displacement

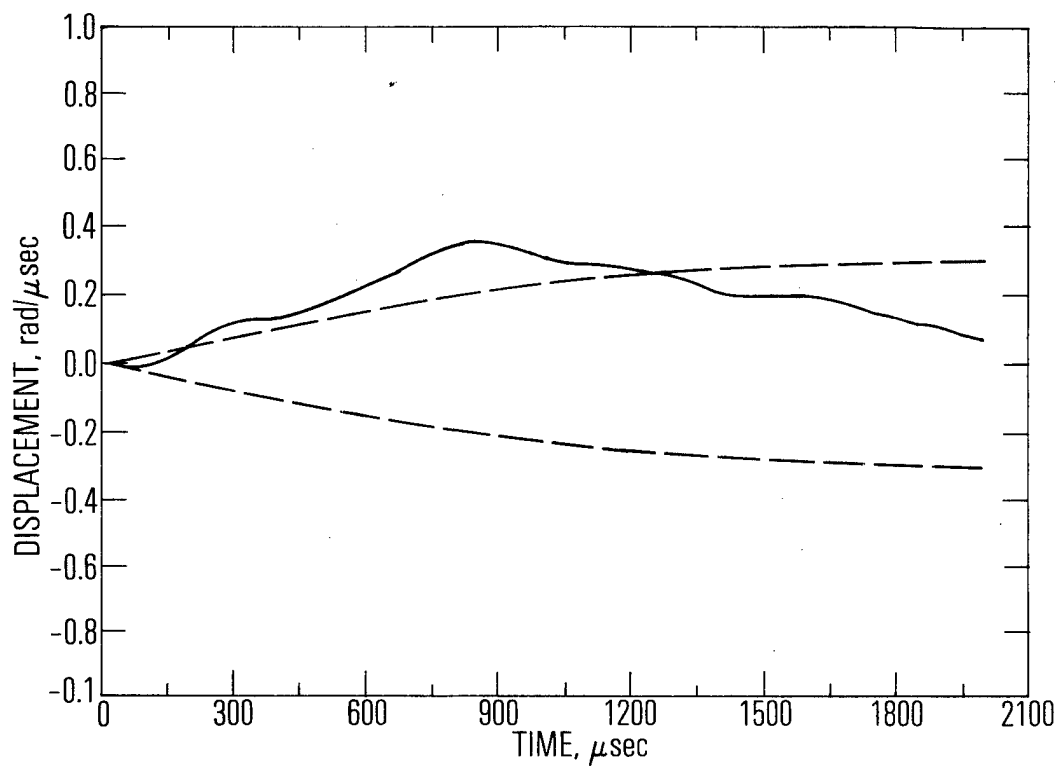


Fig. 12. PZT Displacement Rate

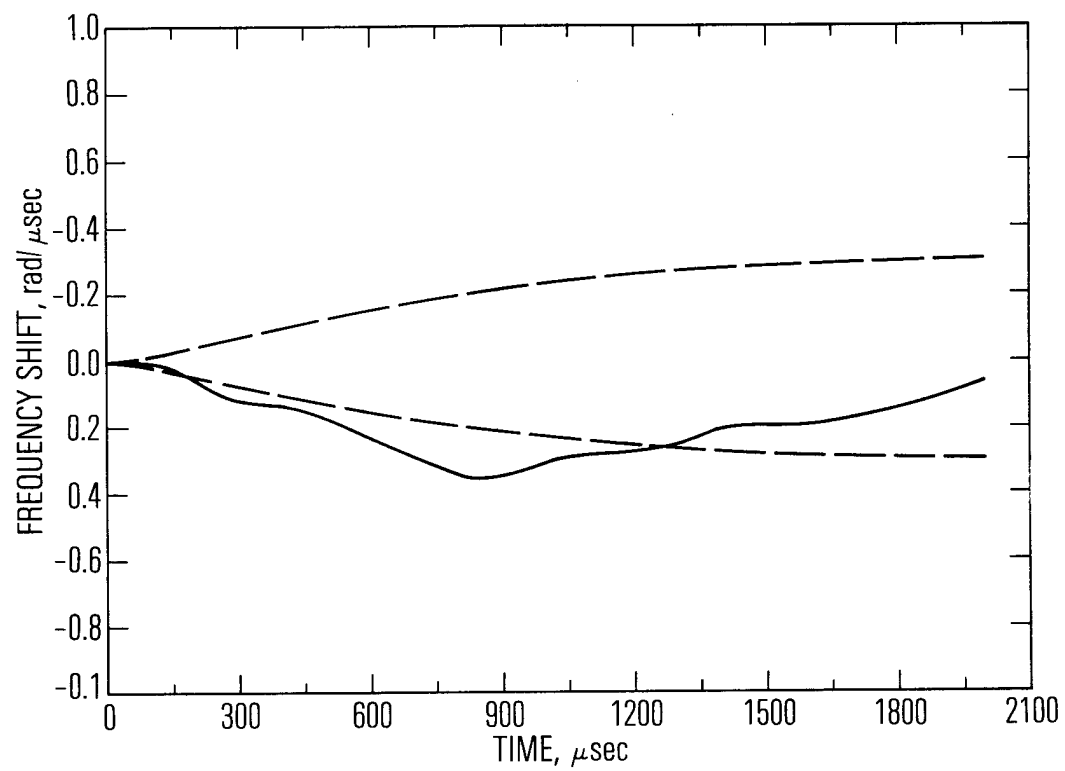


Fig. 13. Laser Frequency Shift

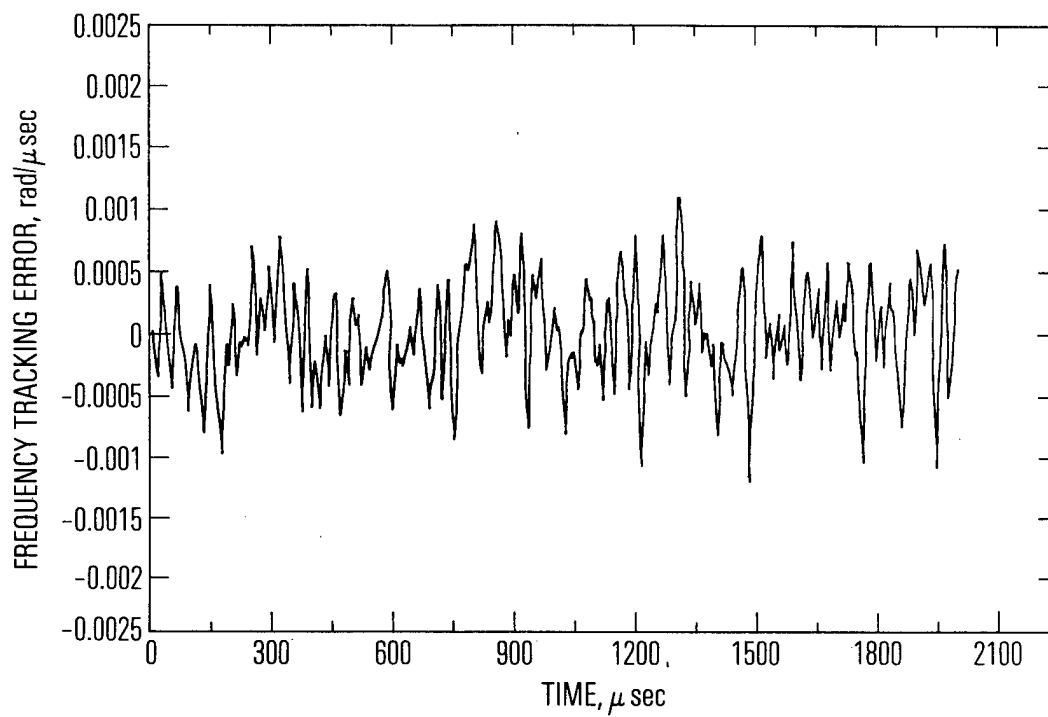


Fig. 14. Frequency Tracking Error

If more refined laser drift measurements require different values of σ or τ or if a different PZT driver requires changes in ζ or ω_n , new control gains and the steady-state RMS phase error can be rapidly determined. Control-system parameter optimization is also possible.

VIII. CONCLUSION

On the bases of the PZT characteristics and the laser frequency drift model derived from experimental data, adequate phase-control of HF chemical lasers appears to be feasible if sensor noise and PZT nonlinearities do not seriously degrade the servo performance. A major improvement over previous laser phase control designs is the use of PZT displacement rate feedback to stabilize and extend the frequency response of the servo.

REFERENCES

1. C. P. Wang, "Master and Slave Oscillator Array System for Very Large Multiline Lasers," *Appl. Opt.* 17, 83-86 (1978).
2. C. L. Hages and L. M. Laughman, "Generation of Coherent Optical Pulses," *Appl. Opt.* 16, 263-264 (1977).
3. J. W. Hardy, "Active Optics: A New Technology for the Control of Light," *Proc. IEEE* 66, 651-697 (1978).
4. J. Munch, M. A. Kolpin, and J. Levine, "Frequency Stability and Stabilization of a Chemical Laser," *IEEE J. Quantum Electron.* QE-14, 17-22 (1978).
5. C. P. Wang, "Frequency Stability of a CW HF Chemical Laser," *J. Appl. Phys.* 47, 221-223 (1976).
6. C. P. Wang and R. L. Varwig, "Frequency Stabilization of HF Lasers by Means of Beat Signals and Anomalous Dispersion," Presented at the Tri-Service Chemical Laser Symposium, Redstone Arsenal, Alabama, 1-3 March 1977.
7. D. J. Spencer, J. A. Beggs, and H. Mirels, "Small-scale CW HF-DF Chemical Laser," *J. Appl. Phys.* 48, 1206-1211 (1977).
8. A. E. Bryson and Y. C. Ho, Applied Optimal Control, Blaisdell, Mass. (1968).
9. M. Athans, "The Role and Use of the Stochastic Linear-Quadratic-Gaussian Problem in Control System Design," *IEEE Trans. Automatic Control*, AC-16, 529-552 (1971).
10. C. P. Wang, "Laser Anemometry," *Am. Sci.* 65, 289-293 (1977).
11. S. A. Davis, Feedback and Control Systems, Simon and Schuster, New York (1974), Chapter 6.
12. C. P. Wang and P. L. Smith, High Frequency PZT Driver by Means of Laser Doppler Sensor and Rate Feedback, ATR-79(8408)-1. The Aerospace Corporation, El Segundo, California (July 1978).
13. W. R. Warren, Jr., "Chemical Lasers," *Aeron. and Astron.* 13, 36-39 (1975).

14. H. Mirels, "Inhomogeneous Broadening Effects in CW Chemical Lasers," (Unpublished).
15. C. P. Wang, and R. L. Varwig, "Longitudinal Mode Beat Intensities in a CW HF Chemical Laser," Appl. Phys. Lett. 29, 345-347 (1976).

APPENDIX A

QUADRATIC SYNTHESIS OF FEEDBACK REGULATOR

A. OPTIMAL CONTROL EQUATIONS

1. PHYSICAL SYSTEM MODEL

$$\dot{\mathbf{x}} = \mathbf{F}\mathbf{x} + \mathbf{G}u$$

2. CONTROLLER

$$u = -\mathbf{C}\mathbf{x}$$

3. PERFORMANCE INDEX

$$J = \frac{1}{2} \int_{t_0}^{t_f} (\mathbf{x}^T \mathbf{A} \mathbf{x} + u^T \mathbf{B} u) dt$$

4. RICCATI EQUATION

$$\dot{\mathbf{S}} = -\mathbf{S}\mathbf{F} - \mathbf{F}^T \mathbf{S} - \mathbf{A} + \mathbf{S}\mathbf{G}\mathbf{B}^{-1}\mathbf{G}^T \mathbf{S}$$

5. OPTIMAL CONTROL GAINS

$$\mathbf{C} = \mathbf{B}^{-1}\mathbf{G}^T \mathbf{S}$$

6. MATRIX DEFINITIONS

$d = s = 0$ by assumption.

$$F = \begin{bmatrix} 0 & 1 & 0 \\ 0 & 0 & 1 \\ 0 & -p_1 & -p_2 \end{bmatrix} \quad G = \begin{bmatrix} 0 \\ 0 \\ p_1 \end{bmatrix}$$

$$A = \begin{bmatrix} W^2 & 0 & 0 \\ 0 & 0 & 0 \\ 0 & 0 & 0 \end{bmatrix} \quad S = \begin{bmatrix} s_{11} & s_{12} & s_{13} \\ s_{12} & s_{22} & s_{23} \\ s_{13} & s_{23} & s_{33} \end{bmatrix}$$

$$B = 1 \quad p_1 = \omega_n^2 \quad p_2 = 2\zeta\omega_n$$

B. STEADY-STATE RICCATI EQUATION COMPONENTS AND OPTIMAL REGULATOR GAINS

$$p_1^2 s_{13}^2 - W^2 = 0$$

$$-2(s_{12} - p_1 s_{23}) + p_1^2 s_{23}^2 = 0$$

$$-2(s_{23} - p_2 s_{33}) + p_1^2 s_{33}^2 = 0$$

$$-(s_{12} - p_2 s_{13}) + p_1^2 s_{13} s_{33} = 0$$

$$-(s_{11} - p_1 s_{13}) + p_1^2 s_{13} s_{23} = 0$$

$$-(s_{22} - p_2 s_{23}) - (s_{13} - p_1 s_{33}) + p_1^2 s_{23} s_{33} = 0$$

C. SOLUTION TO STEADY-STATE RICCATI EQUATION

$$s_{13} = \frac{W}{p_1}$$

$$\frac{p_1^6}{4} s_{33}^4 + p_1^4 p_2 s_{33}^3 + (p_1^2 p_2^2 + p_1^3) s_{33}^2 + 2(p_1 p_2 - p_1 W) s_{33} - 2 \frac{p_2}{p_1} W = 0$$

solved numerically for positive real root and plotted in Fig. A-1.

$$s_{23} = \frac{p_1^2 s_{33}^2 + 2 p_2 s_{33}}{2}$$

$$s_{12} = \frac{p_2}{p_1} W + p_1 W s_{33}$$

$$s_{11} = W + p_1 W s_{23}$$

$$s_{22} = p_2 s_{23} - \frac{W}{p_1} + p_1 s_{33} + p_1^2 s_{22} s_{33}$$

D. REGULATOR GAINS

The rate loop gain C_3 is only a function of ζ , ω_n , and W and is given in normalized form in Fig. A-1. The gains for any W , ω_n , and ξ can be determined with the use of C_3 in Fig. A-1 and by solving for C_1 and C_2 by means of the control-gain expressions.

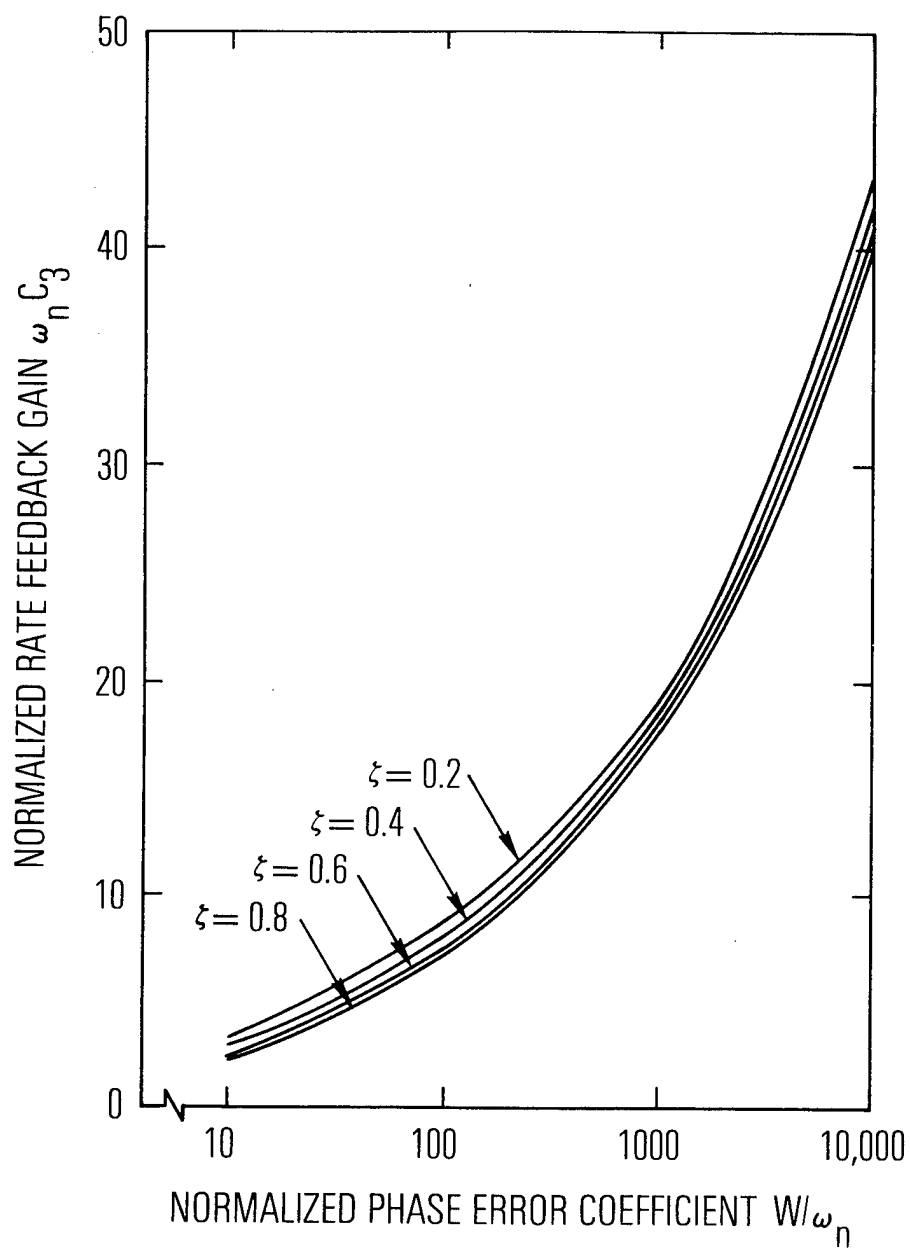


Fig. A-1. Rate Feedback Gain

$$C_1 = p_1 s_{13} = W$$

$$C_2 = p_1 s_{23} = \frac{p_1 C_3^2 + 2p_2 C_3}{2}$$

$$C_3 = p_1 s_{33}$$

APPENDIX B

STEADY-STATE COVARIANCE OF STATE VECTOR

A. COVARIANCE EQUATIONS

1. PHYSICAL SYSTEM MODEL

$$\dot{\mathbf{x}} = (\mathbf{F} - \mathbf{GC})\mathbf{x} + \mathbf{r}$$

2. NOISE MODEL

$$\mathbf{E}[\mathbf{r}] = 0$$

$$\mathbf{E}[\mathbf{r}(t)\mathbf{r}(t + \tau)] = \mathbf{Q}\delta(\tau)$$

3. COVARIANCE OF \mathbf{x}

$$\mathbf{X} = \text{cov}[\mathbf{x}]$$

$$\dot{\mathbf{X}} = \mathbf{A}\mathbf{X} + \mathbf{X}\mathbf{A}^T + \mathbf{Q}$$

4. MATRIX DEFINITIONS

$$\mathbf{x}^T = (\theta \quad y \quad v \quad s \quad d)$$

$$\mathbf{A} = \begin{bmatrix} 0 & 1 & 0 & 0 & 1 \\ 0 & 0 & 1 & 0 & 0 \\ -a_1 & -a_2 & -a_3 & 0 & -a_4 \\ 0 & 0 & 0 & -p_3 & 0 \\ 0 & 0 & 0 & p_3 & -p_3 \end{bmatrix}$$

$$X = \begin{bmatrix} x_{11} & x_{12} & x_{13} & x_{14} & x_{15} \\ x_{12} & x_{22} & x_{23} & x_{24} & x_{25} \\ x_{13} & x_{23} & x_{33} & x_{34} & x_{35} \\ x_{14} & x_{24} & x_{34} & x_{44} & x_{45} \\ x_{15} & x_{25} & x_{35} & x_{45} & x_{55} \end{bmatrix}$$

$$Q = \begin{bmatrix} 0 & 0 & 0 & 0 & 0 \\ 0 & 0 & 0 & 0 & 0 \\ 0 & 0 & p_1^2 q & 0 & 0 \\ 0 & 0 & 0 & 2p_3 \sigma^2 & 0 \\ 0 & 0 & 0 & 0 & 0 \end{bmatrix}$$

$$a_1 = p_1 C_1 \quad a_2 = p_1 (C_2 + 1) \quad a_3 = p_2 + p_1 C_3 \quad a_4 = p_1 C_2$$

B. SIMULTANEOUS LINEAR EQUATIONS FOR
STEADY-STATE COVARIANCE

$$2x_{12} + 2x_{15} = 0$$

$$x_{22} + x_{25} + x_{13} = 0$$

$$x_{23} + x_{35} - a_1 x_{11} - a_2 x_{12} - a_3 x_{13} - a_4 x_{15} = 0$$

$$x_{24} + x_{45} - p_3 x_{14} = 0$$

$$x_{25} + x_{55} + p_3(x_{14} - x_{15}) = 0$$

$$2x_{23} = 0$$

$$x_{33} - a_1 x_{12} - a_2 x_{22} - a_3 x_{23} - a_4 x_{25} = 0$$

$$x_{34} - p_3 x_{24} = 0$$

$$x_{35} + p_3(x_{24} - x_{25}) = 0$$

$$-2(a_1 x_{13} + a_2 x_{23} + a_3 x_{33} + a_4 x_{35}) + p_1^2 q = 0$$

$$-a_1 x_{14} - a_2 x_{24} - a_3 x_{34} - a_4 x_{45} - p_3 x_{34} = 0$$

$$p_3(x_{34} - x_{35}) - a_1 x_{15} - a_2 x_{25} - a_3 x_{35} - a_4 x_{55} = 0$$

$$-2p_3 x_{44} + 2p_3 \sigma^2 = 0$$

$$-2p_3 x_{45} + p_3 x_{44} = 0$$

$$2p_3(x_{45} - x_{55}) = 0$$

C. SOLUTION TO STEADY-STATE COVARIANCE

This closed-form solution was derived and computer checked by C. M. McKenzie. (The solution extends beyond the formulation given in the text to include a white noise input with power spectral density q .)

$$x_{23} = 0$$

$$x_{44} = \sigma^2$$

$$x_{45} = \frac{\sigma^2}{2} = \frac{x_{44}}{2}$$

$$x_{55} = \frac{\sigma^2}{2} = x_{45}$$

$$x_{14} = \frac{\sigma^2(p_3^2 + a_3p_3 + a_2 - a_4)}{2(p_3^3 + a_3p_3^2 + a_2p_3 + a_1)}$$

$$x_{24} = p_3x_{14} - \frac{\sigma^2}{2}$$

$$x_{34} = p_3x_{24}$$

$$x_{15} = \frac{x_{14}(p_3^3 + a_3p_3^2 + a_2p_3) + a_{24}(2p_3^2 + a_3p_3) + x_{55}(a_3p_3 + p_3^2 + a_2 - a_4)}{p_3^3 + a_3p_3^2 + a_2p_3 + a_1}$$

$$x_{25} = p_3(x_{15} - x_{14}) - x_{55}$$

$$x_{35} = p_3(x_{25} - x_{24})$$

$$x_{12} = -x_{15}$$

$$x_{13} = \frac{\frac{p_1^2 q}{2} - a_1 a_3 x_{12} - a_4 x_{35} + a_3 x_{25}(a_2 - a_4)}{a_1 - a_2 a_3}$$

$$x_{22} = -x_{25} - x_{13}$$

$$x_{33} = a_1 x_{12} + a_2 x_{22} + a_4 x_{25}$$

$$x_{11} = \frac{x_{35} - a_2 x_{12} - a_3 x_{13} - a_4 x_{15}}{a_1}$$

DISTRIBUTION

Internal

J. M. Bernard	W. F. Leverton
J. F. Bott	P. Mahadevan
R. A. Chodsko	H. Mirels
N. Cohen	G. A. Paulikas
E. F. Cross	W. C. Riley
D. A. Durran	S. Siegel
J. W. Ellinwood	A. H. Silver
M. Epstein	D. J. Spencer
R. R. Giedt	D. G. Sutton
W. A. Griesser	B. L. Taylor
R. W. F. Gross	T. D. Taylor
R. A. Hartunian	E. B. Turner
T. S. Hartwick	R. L. Varwig
R. F. Heidner	C. P. Wang
J. M. Herbelin	W. R. Warren, Jr.
D. T. Hodges, Jr.	K. R. Westberg
R. Hofland, Jr.	J. S. Whittier
J. J. T. Hough	M. T. Weiss
M. A. Kwok	R. L. Wilkins

External

SAMSO

Lt. Col. Lindemuth (YCPT)
Lt. A. Fernandez (YCPT)
Lt. Col. J. R. Doughty (YD)
Mr. G. E. Aichinger (TM)

AFWL

Kirtland AFB, NM 87117
Col. J. Rich (AR)
Lt. Col. A. D. Maio (AL)
Dr. P. Avizonis (AL)
Capt. B. Crane (ALC)
Dr. L. Wilson (ALC)
Maj. D. Olson (ALC)
Mr. L. Rapagnani (ALC)

DARPA

1400 Wilson Boulevard
Arlington, VA 22209
Dr. H. A. Pike
Dr. J. Mangano

AVCO-Everett Research Laboratory

2385 Revere Beach Parkway
Everett, MA 02149
Dr. G. W. Sutton
Dr. J. Dougherty

Science Applications, Inc.
P.O. Box 328
5 Research Drive
Ann Arbor, MI 48105
Dr. R. E. Meredith

Science Applications, Inc.
2361 Jefferson Davis Highway
Arlington, VA 22202
Dr. W. R. Sooy

Lawrence Livermore Laboratory
P.O. Box 808
Livermore, CA 94550
Dr. J. Emmett
Dr. A. Karo

Arnold Engineering Development
Center
Arnold Air Force Station, TN 37389
L.R. Case (XOOE)

ODUS DRE (R&AT)
The Pentagon
Washington, DC 20301
Dr. G. P. Millburn, Rm 3E114

Deputy Undersecretary of Defense
Tactical Warfare Programs
The Pentagon
Washington, DC 20301
Mr. R. A. Moore, Rm 3E1044

Deputy Undersecretary of Defense
The Pentagon
Washington, DC 20301
Dr. S. Zeiberg, Rm 3E130

TRW Systems Group
One Space Park
Redondo Beach, CA 90278
Dr. J. Miller, 01/1080
Dr. D. Bullock
Dr. J. Stansel
Dr. C. W. Clendening, Jr.,
Bldg. R1, Rm 1016
Dr. P. Clark

United Technologies Research
Laboratories
400 Main Street
East Hartford, CT 06108
Dr. J. Hinchey
Dr. A. Angelbeck
Dr. D. Seery
Dr. C. Ultee

University of Maryland
College Park, MD 20740
College of Engineering
Department of Aerospace
Engineering
Dr. J. D. Anderson, Jr.

Wright State University
Dayton, OH 45431
Department of Chemistry
Dr. T. O. Tiernan
Dr. G. D. Sides

University of Southern California
Los Angeles, CA 90007
Department of Chemistry
Prof. S. W. Benson
Department of Electrical
Engineering
Prof. C. Wittig

University of California, San Diego
La Jolla, CA 92703
Department of AMES
Prof. S. S. Penner
Prof. S. C. Lin

University of Arizona
Tucson, AZ 85721
College of Liberal Arts
Department of Physics
Dr. G. Khayrallah, Bldg 181

IRIA Center
ERIM
P.O. Box 8618
Ann Arbor, MI 48107

Bell Aerospace Textron
P.O. Box 1
Buffalo, NY 14240
Dr. W. Solomon, Mail Zone B-49
Dr. J. Blauer, Mail Zone B-49
Dr. J. W. Raymonda,
Mail Zone B-49
Dr. R. J. Driscoll,
Mail Zone B-49

California Institute of Technology
Pasadena, CA 91109
Prof. A. Kuppermann
Prof. H. Liepmann
Prof. A. Roshko

CALSPAN Corporation
P.O. Box 235
Buffalo, NY 14221
Dr. J. Daiber
Dr. C. E. Treanor

AFRPL (LKCG)
Edwards AFB, CA 93523
B. R. Bornhorst

Columbia University
Department of Chemistry
New York, NY 10027
Dr. R. Zare

Michigan State University
E. Lansing, MI 48824
Department of Mechanical
Engineering
Dr. R. Kerber

Cornell University
Ithaca, NY 14853
Department of Applied Physics
Dr. T. A. Cool
Department of Chemistry
Dr. S. H. Bauer

Hughes Research Laboratory
3011 Malibu Canyon Road
Malibu, CA 90265
Dr. A. Chester

Los Alamos Scientific Laboratory
Los Alamos, NM 87545
Dr. K. Boyer
Dr. E. Brock
Dr. G. Emanuel
Dr. R. Jensen
Dr. E. O'Hair
Dr. J. Parker, Mail Station
Dr. S. Rockwood

Deputy Chief of Staff for
Research, Development and
Acquisition
Department of the Army Headquarters
The Pentagon
Washington, DC 20310
Lt C. B. J. Pellergrini, 3B482

US Army Missile Research and
Development Command
Redstone Arsenal, AL 35809
Mr. J. M. Walters (DRDMI-HS)
Dr. W. Wharton (DRSMI-RK)
Dr. T. A. Barr, Jr (DRSMI-RH)
Dr. D. Howgate

General Electric Company
U7211 VFSTC
P.O. Box 8555
Philadelphia, PA 19101
R. Geiger
J. Gilstein

Deputy Assistant Secretary of the
Navy
Research and Advanced Technology
The Pentagon
Washington, DC 20350
Dr. T. A. Jacobs, Rm 4D 745
Dr. R. Hoglund, Rm 4D 745

Naval Research Laboratory
4550 Overlook Avenue SW
Washington, DC 20375
Dr. W. S. Watt, Code 5540
Dr. J. M. MacCallum,
Code 5503 EOTP
Dr. S. K. Searles, Code 5540

Naval Sea Systems Command
Washington, DC 20362

Dr. D. Finkleman, PMS-405-20
Dr. L. Stoessell, PMS-405-30
Dr. J. A. Stregack, PMS-405-23
Capt. A. Skolnick, PMS-405

Hughes Aircraft Company
Centinella and Teal Street
Culver City, CA 90230
Dr. E. R. Peressini
Dr. M. Mann

Lockheed Missiles and Space Company
P.O. Box 1103, West Station
Huntsville, AL 35807
Dr. S. C. Kurzius

Lockheed Missiles and Space Company
4800 Bradford Blvd.
Huntsville, AL 35812
J. W. Benefield

Martin-Marietta
Denver, CO 80202
Dr. J. Bunting

Massachusetts Institute of Technology
Cambridge, MA 02139
Department of Physics
Dr. A. Javan
Department of Chemistry
Dr. J. Steinfeld

Naval Surface Weapons Center
White Oak Laboratory
Silver Springs, MD 20910
Dr. E. L. Harris,
Code WA-13, Bldg 405, Rm 219

Commander
Naval Weapons Center
China Lake, CA 93555
E. Lunstrom, Code 4011
H. E. Bennett

NASA Lewis Research Center
21000 Brook Park Road
Cleveland, OH 44135
S. Cohen, Mail Station 500-209

NASA Ames Research Center
Moffett Field, CA 94035
Dr. C. F. Hansen

Mathematical Sciences Northwest,
Inc.
P.O. Box 1887
Bellevue, WA 98009
Dr. S. Byron
Prof. A. Hertzberg
P. Rose
Dr. R. Center

McDonnell Douglas Corporation
5301 Bolsa Avenue
Huntington Beach, CA 92647
Dr. R. Lee, Bldg. 28, Rm 250
Dr. W. A. Gaubatz

McDonnell Research Laboratory
McDonnell Douglas Corporation
St. Louis, MO 63166
Dr. D. P. Ames
Dr. R. Haakinen
Dr. D. Kelly

Northrop Corporation
Research and Technology Center
1 Research Park
Palos Verdes Peninsula, CA 90274
Dr. M. L. Bhaumik

RADC/ETSL
Hanscom Air Force Base, MA 01731
Dr. H. Schlossberg

AFSC (DLS)
Andrews AFB
Washington, DC 20334

AFML (NA)
Wright-Patterson AFB, OH 45433

Air University Library
Maxwell AFB, AL 36112

Air Force Office of Scientific Research
Bolling AFB, DC 20332
Directorate of Aerospace
Sciences (NA)
Directorate of Physics (NP)
Capt. Russell Armstrong

Perkin-Elmer Corporation
Norwalk, CN 06856
Electro-Optical Division
M. L. Skolnick

Physics International Company
2700 Merced Street
San Leandro, CA 94577
Dr. B. Bernstein

Pratt and Whitney Aircraft Corporation
P.O. Box 2691
West Palm Beach, FL 33402
Dr. G. H. McLafferty,
Mail Station B47
Mr. R. Oglukian,
Mail Station B47

Princeton University
Princeton, NJ 08540
Department of Aerospace and
Mechanical Science
Prof. S. Bogdonoff

Rockwell International Corporation
Science Center
1049 Camino Dos Rios
Thousand Oaks, CA 91360
Dr. A. T. Pritt, Jr.

FJSRL (Tech Library)
USAF Academy, CO 80840

Scientific and Technical Information
Facility
P.O. Box 33
College Park, MD 20740
NASA Representative

RADC (XP)
Griffiss AFB, NY 13442

Electric Power Research Institute
P.O. Box 10412
Palo Alto, CA 94303
Dr. W. Gough
Dr. N. Amhert

Department of Energy
Washington, DC 20545
Division of Laser Fusion
Dr. C. M. Stickley, Director
Dr. Paul Hoff
Dr. J. Weiss
Nuclear Research and Application
Advanced Isotope Separation
Technology
Dr. K. Hancock, Mail Station
Mail Station H407

Purdue University
School of Mechanical Engineering
Chaffee Hall
Lafayette, IN 47907
Prof. J. G. Skifstad

Rockwell International Corporation
Rocketdyne Division
Canoga Park, CA 91304
Dr. S. V. Gunn
Dr. A. Axworthy
Dr. E. Curtis
Dr. L. Zajac

BDM Corporation
2600 Yale Boulevard SE
Albuquerque, NM 87106
Dr. R. Rose

W. J. Schafer Associates, Inc.
901 N. Fort Myer Drive, Suite 803
Arlington, VA 22209
Dr. E. T. Gerry
Dr. W. Evers

W. J. Schafer Associates, Inc.
10 Lakeside Office Park
Wakefield, MA 01880
Dr. J. Reilly